(Received 14 April 2026, Accepted 8 May 2026, Scheduled 14 May 2026)

# A Unified Conformal FDTD Formulation Based on Harmonic Mean Weighting for Dielectric and PEC Objects

Cuihua Li[1], Haofeng Wang[1], Jun Zheng[1], and Minquan Li[2,*]

[1] *School of Electronic Information and Automation Hefei University, Hefei, China*
[2] *Information Materials and Intelligent Sensing Laboratory of Anhui Province, Anhui University, Hefei 230601, China*

**ABSTRACT:** To address the need to differentiate between dielectric and perfect electric conductor (PEC) conformal methods in the finite-difference time-domain (FDTD), this study proposes a conformal approach based on the harmonic mean to achieve a unified formulation. In this approach, the relevant electromagnetic parameters are weighted using harmonic mean weighting, enabling a conformal implementation within the FDTD framework. Both dielectric and PEC conformality are incorporated into a single mathematical framework, allowing for a unified treatment in the FDTD. The proposed method provides a consistent formulation that can be seamlessly integrated with standard FDTD procedures while ensuring high compatibility and accuracy of the results. The conformal method based on harmonic mean requires only 60% of the computational time and 36% of the memory compared to the CST, indicating its high computational efficiency. Furthermore, it demonstrates strong applicability to complex biological models, such as specific absorption rate (SAR) calculations in the human head. This approach is particularly well-suited for RF device design and biomedical applications, offering improved modeling efficiency and reliability.

## 1. INTRODUCTION

In electromagnetic performance simulations, discretization is an indispensable step. The finite-difference time-domain (FDTD) method is a widely used numerical technique in computational electromagnetics [1, 2]. Although the Yee grid provides an effective means of spatial discretization, it inevitably introduces staircasing errors [3].

Conformal techniques have been developed to mitigate the staircasing errors resulting from the FDTD mesh discretization. Dey and Mittra proposed weighting the electric and magnetic fields in the FDTD iterative formulas according to the proportion of each material within a grid cell [4]. This approach is intuitive and can significantly improve accuracy; however, it requires modifications to the iterative formulas, which complicates implementation. Alternative methods achieve conformality by performing auxiliary evaluations of cells near the conformal boundary [5]. Although these methods can achieve high accuracy, they are relatively complex to implement in practice. Some researchers further subdivide conformal cells into subregions corresponding to different materials, compute the electric and magnetic fields separately for each subregion, and then combine the results to obtain the field quantities for the entire cell [6, 7]. Although these approaches are accurate, they incur high computational cost and implementation complexity.

To further enhance the accuracy, electric field weighting was extended to incorporate not only the proportion of material along the grid edges but also an area factor. These approaches originate from the finite-volume method and have gradually been adopted in conformal FDTD techniques [8, 9]. For specific models or to accelerate computations, some studies have integrated conformal techniques with implicit FDTD schemes [10, 11].

To balance the accuracy and implementation complexity, conformal methods based on weighting the constitutive parameters have been proposed [12, 13]. These methods are applicable to both dielectric and perfect electric conductor (PEC) conformality and can be readily integrated within the FDTD framework. However, their formulations must be applied differently depending on the situation, resulting in a lack of uniformity and making the formulas less intuitive for systematic understanding.

Currently, the remaining challenges can be summarized as follows: 1) Conformal implementation typically requires classification into dielectric and PEC conformal methods, with the iterative formulas for each category differing and needing to be treated separately. 2) Using the arithmetic mean to weight the constitutive parameters leads to formulations that are incomplete and lack clarity, reducing readability and interpretability. 3) Metals are characterized by high electrical conductivity, and metallic conformality is often approximated as PEC conformality; that is, metals are directly treated as PEC. This approximation becomes problematic when multiple types of metals with distinct electromagnetic properties are present, complicating accurate conformal treatment.

To address these challenges, the main contributions of this study are summarized as follows: 1) The conformal implementation no longer requires separate classification; the iterative formulas for dielectric and PEC conformality are unified within a single framework. 2) Harmonic mean weighting is employed instead of the arithmetic mean to improve the accuracy and

* Corresponding author: Minquan Li (limq@ahu.edu.cn).

completeness of the constitutive parameter representation. 3) Metallic conformality is no longer approximated as PEC conformality, allowing the actual electromagnetic parameters of metals to be directly incorporated into conformal formulations.

## 2. FORMULATIONS

The FDTD method is founded on Maxwell's equations.

$$\begin{aligned} \nabla \times \mathbf{H} &= \frac{\partial \mathbf{D}}{\partial t} + \mathbf{J}, \\ \nabla \times \mathbf{E} &= -\frac{\partial \mathbf{B}}{\partial t} - \mathbf{M}, \end{aligned} \tag{1}$$

where **E** is the electric field intensity, **D** the electric flux density (electric displacement field), **H** the magnetic field intensity, **B** the magnetic flux density, **J** the current density, **M** the magnetic current density, and $t$ the time.

The use of the Yee grid for spatial discretization in the FDTD method inevitably introduces staircasing error. The parameter-weighting approach proposed in [12] effectively alleviates these errors. Conformal techniques are generally classified into dielectric conformal and PEC conformal methods, which employ distinct formulations to achieve geometric conformity.

The core of the conformal implementation involves weighting the dielectric constant $\varepsilon$ and electrical conductivity $\sigma$ in the electric field according to the fraction of the grid edge occupied by each material. For the magnetic field, the magnetic permeability $\mu$ and magnetic loss coefficient $\sigma_m$ are weighted based on the area fraction of the material within the grid cell, where $\sigma_m$ is introduced to preserve symmetry in Maxwell's equations.

### 2.1. Dielectric Conformal Method

In Fig. 1, $A$, $B$, $C$, and $D$ represent the four edges of a grid cell, while $F$ denotes the location of the magnetic field at the cell center. $\Delta x$ and $\Delta y$ correspond to the lengths of a single grid cell in the $x$ and $y$ directions, respectively. $S_{xy1}$ and $S_{xy2}$ represent the areas of the grid cell occupied by medium 1 and medium 2, respectively. $l_{x1}$ and $l_{y1}$ denote the lengths of the edges occupied by medium 1, whereas $l_{x2}$ and $l_{y2}$ denote those occupied by medium 2. The subscripts $x$, $y$, and $z$ of the physical quantities $\varepsilon$, $\sigma$, $\mu$, and $\sigma_m$ indicate their respective components along the $x$, $y$, and $z$ directions.

The parameter-weighting approach is applied to the electric field, as shown in (2) and (3).

$$\begin{cases} \varepsilon_x^{eff}(A) = [l_{x1} \cdot \varepsilon_1 + l_{x2} \cdot \varepsilon_2]/\Delta x, \\ \varepsilon_y^{eff}(B) = \varepsilon_1, \\ \varepsilon_x^{eff}(C) = \varepsilon_1, \\ \varepsilon_y^{eff}(D) = [l_{y1} \cdot \varepsilon_1 + l_{y2} \cdot \varepsilon_2]/\Delta y. \end{cases} \tag{2}$$

$$\begin{cases} \sigma_x^{eff}(A) = [l_{x1} \cdot \sigma_1 + l_{x2} \cdot \sigma_2]/\Delta x, \\ \sigma_y^{eff}(B) = \sigma_1, \\ \sigma_x^{eff}(C) = \sigma_1, \\ \sigma_y^{eff}(D) = [l_{y1} \cdot \sigma_1 + l_{y2} \cdot \sigma_2]/\Delta y. \end{cases} \tag{3}$$

The parameter-weighting approach is applied to the magnetic field in (4).

$$\begin{aligned} \mu_z^{eff}(F) &= [S_{xy1} \cdot \mu_1 + S_{xy2} \cdot \mu_2]/\Delta x \Delta y, \\ \sigma_{mz}^{eff}(F) &= [S_{xy1} \cdot \sigma_{m1} + S_{xy2} \cdot \sigma_{m2}]/\Delta x \Delta y. \end{aligned} \tag{4}$$

### 2.2. PEC Conformal Technique

In the PEC conformal method, the core principle is that the PEC regions are assumed to require no processing. Fig. 2 illustrates the equivalent approach for implementing PEC conformality in the proposed design.

The parameter-weighting method for the electric field in the PEC regions is shown in (5) and (6).

$$\begin{cases} \varepsilon_x^{eff}(A) = \varepsilon_1, \\ \varepsilon_y^{eff}(B) = \varepsilon_1, \\ \varepsilon_x^{eff}(C) = \varepsilon_1, \\ \varepsilon_y^{eff}(D) = \varepsilon_1. \end{cases} \quad \begin{cases} \sigma_x^{eff}(A) = \sigma_1, \\ \sigma_y^{eff}(B) = \sigma_1, \\ \sigma_x^{eff}(C) = \sigma_1, \\ \sigma_y^{eff}(D) = \sigma_1. \end{cases} \tag{5}$$

Parameter-weighting method for the magnetic field in PEC regions is shown in (6).

$$\mu_z^{eff}(F) = \mu_1, \quad \sigma_{mz}^{eff}(F) = \sigma_{m1}. \tag{6}$$

### 2.3. Conformal Method using the Harmonic Mean

Equations (2)–(4), which implement the dielectric conformal method, employ arithmetic averaging for parameter weighting. Equations (5) and (6) implement PEC conformality by directly treating the PEC regions as requiring no modification, which can reduce clarity and hinder readability. In this study, a harmonic mean weighting approach is proposed for electromagnetic parameters. This method unifies the weighting formulas for both dielectric and PEC regions, eliminating the need to distinguish between them. In practical engineering applications, where most devices are composed of multiple materials, harmonic mean weighting enables a single update of the parameters without applying different formulas to different regions of the device. Furthermore, it enhances the clarity and interpretability of these formulations. The results obtained using harmonic mean weighting, namely (7)–(9), are consistent with those derived from (2)–(6).

Even for metals, variations in material parameters between different metals can be significant. For distinct metals, their actual parameters can be directly applied in the formulas rather than defaulting all metals to PEC. Fig. 3 illustrates an equivalent

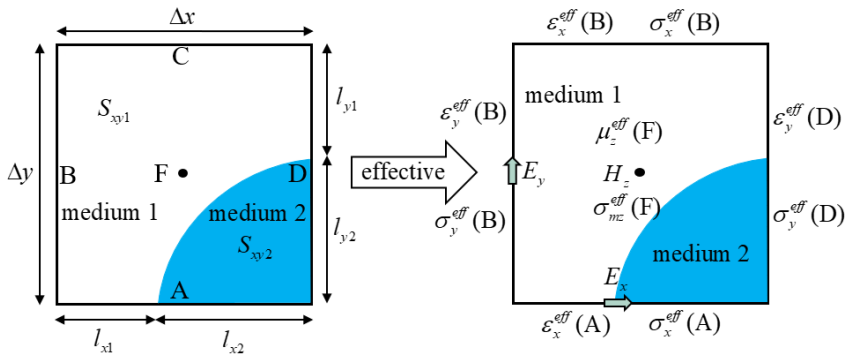


**FIGURE 1**. An equivalent approach for implementing dielectric conformal techniques.

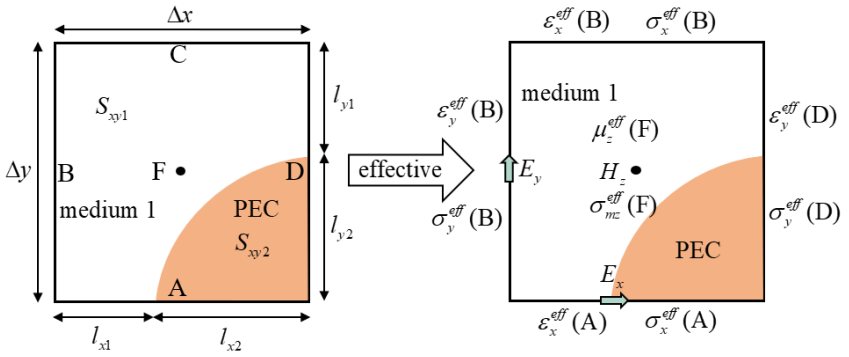


**FIGURE 2**. An equivalent method for implementing the parameter-weighting approach in regions containing PEC.

schematic of the conformal implementation using the harmonic mean.

The unified formulation for weighting the electric field parameters in conformal implementations is given by (7) and (8).

$$\begin{cases} \varepsilon_x^{eff}(A) = \left[\dfrac{l_{x1}/\Delta x}{\varepsilon_1} + \dfrac{l_{x2}/\Delta x}{\varepsilon_2}\right]^{-1}, \\ \varepsilon_y^{eff}(B) = \left[\dfrac{1}{\varepsilon_1}\right]^{-1}, \\ \varepsilon_x^{eff}(C) = \left[\dfrac{1}{\varepsilon_1}\right]^{-1}, \\ \varepsilon_y^{eff}(D) = \left[\dfrac{l_{y1}/\Delta y}{\varepsilon_1} + \dfrac{l_{y2}/\Delta y}{\varepsilon_2}\right]^{-1}. \end{cases} \tag{7}$$

$$\begin{cases} \sigma_x^{eff}(A) = \left[\dfrac{l_{x1}/\Delta x}{\sigma_1} + \dfrac{l_{x2}/\Delta x}{\sigma_2}\right]^{-1}, \\ \sigma_y^{eff}(B) = \left[\dfrac{1}{\sigma_1}\right]^{-1}, \\ \sigma_x^{eff}(C) = \left[\dfrac{1}{\sigma_1}\right]_1^{-1}, \\ \sigma_y^{eff}(D) = \left[\dfrac{l_{y1}/\Delta y}{\sigma_1} + \dfrac{l_{y2}/\Delta y}{\sigma_2}\right]^{-1}. \end{cases} \tag{8}$$

The unified parameter-weighting formulation for the magnetic field in conformal implementations is given by (9).

$$\begin{aligned} \mu_z^{eff}(F) &= \left[\frac{S_{xy1}/\Delta x\Delta y}{\mu_1} + \frac{S_{xy2}/\Delta x\Delta y}{\mu_2}\right]^{-1}, \\ \sigma_{mz}^{eff}(F) &= \left[\frac{S_{xy1}/\Delta x\Delta y}{\sigma_{m1}} + \frac{S_{xy2}/\Delta x\Delta y}{\sigma_{m2}}\right]^{-1}. \end{aligned} \tag{9}$$

The harmonic mean-based conformal approach can naturally accommodate both PEC and dielectric materials. Notably, in extreme cases such as when $\sigma$ approaches infinity or $\varepsilon$ approaches a limiting value, no separate conditional formulations are required.

The conformal implementation based on the harmonic mean allows a one-step update without distinguishing between the dielectric and PEC conformality. Fig. 4 presents a flowchart of the FDTD procedure for conformal implementation using the harmonic mean.

## 3. NUMERICAL EXAMPLES

Two benchmark examples are presented in this study to validate the accuracy of the harmonic mean weighting method. The first is a copper sphere, which demonstrates that the harmonic mean and arithmetic mean approaches yield consistent results. The second example is a human head model composed of multiple dielectric materials. All simulations were performed on a computer equipped with an Intel 12th-generation Core i7-

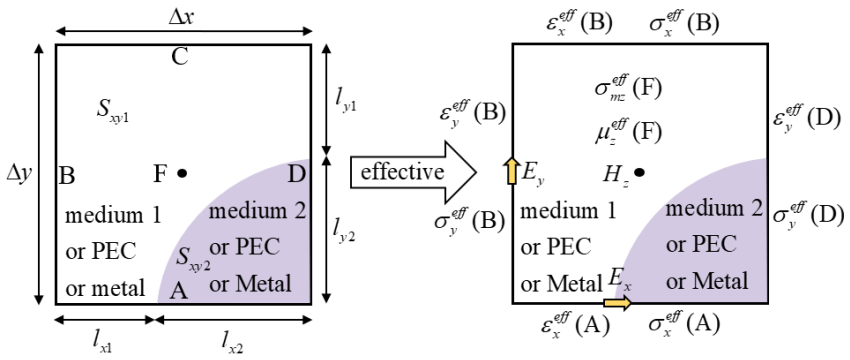


**FIGURE 3**. Conformal implementation using the harmonic mean.

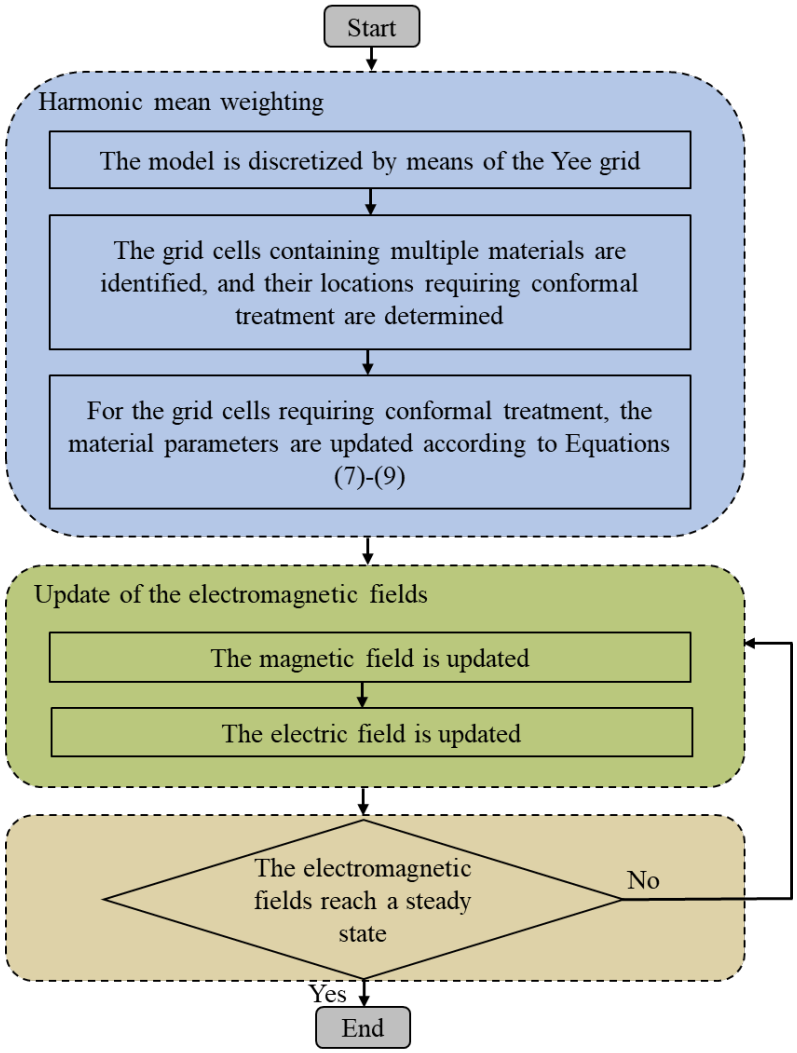


**FIGURE 4**. Flowchart of the FDTD procedure for conformal implementation based on harmonic mean weighting.

12700 processor (12 cores, 2.1 GHz) and 64 GB of 2133 MHz DDR4 memory.

### 3.1. Model of a Copper Sphere

To validate the accuracy and effectiveness of the harmonic mean-based conformal method, a copper sphere was employed as a benchmark example. The radius of the sphere was 10 cm, and the spatial discretization was set to $\Delta x = \Delta y = \Delta z = 15$ mm. An 8-layer convolutional perfectly matched layer (CPML) was applied as the absorbing boundary condition. The material properties of copper were specified as relative permittivity $\varepsilon_r = 1$, permeability $\mu_r = 1$, and electrical conductivity $\sigma = 5.8 \times 10^7$ S/m.

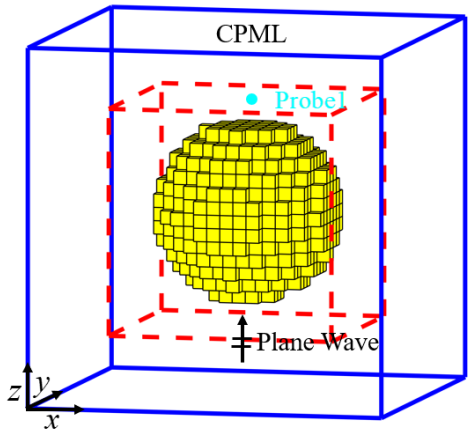


**FIGURE 5**. Copper sphere model.

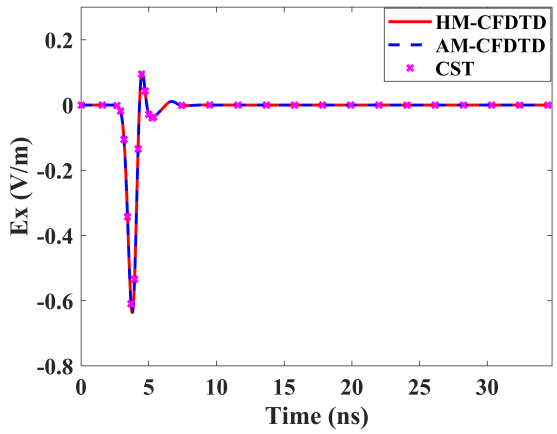


**FIGURE 6**. Time evolution of the electric field $E_x$ at Probe1 for the three methods.

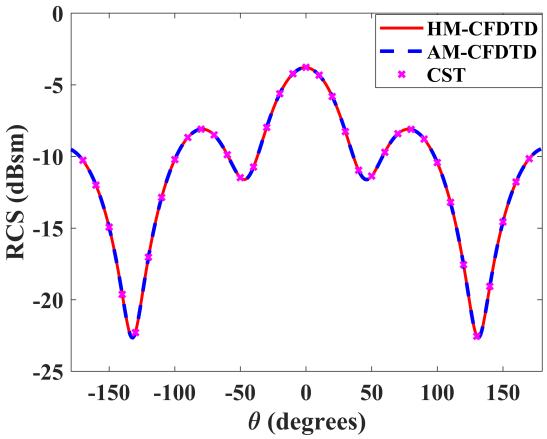


**FIGURE 7**. RCS in the $x$-$z$ plane.

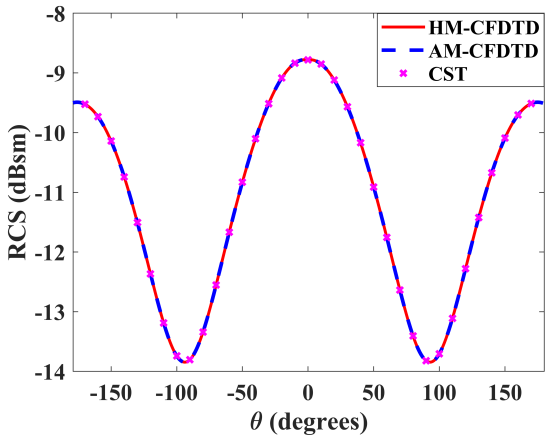


**FIGURE 8**. RCS in the $x$-$y$ plane.

Because conformality is implemented using harmonic-mean weighting, the physical parameters appear in the denominator and therefore cannot be zero. In conventional treatments, the electrical conductivity of air is often assumed to be zero; however, this is only an approximation rather than the true physical value. In this study, the actual conductivity of air is adopted, thereby satisfying this requirement. The material properties of air were specified as $\varepsilon_r = 1$, $\mu_r = 1$, and $\sigma = 1 \times 10^{-12}$ S/m. Fig. 5 shows the mesh discretization of the copper spheres. A Gaussian pulse plane wave was employed as the excitation source, as defined in (10), with polarization along the $x$-direction.

$$g(t) = Me^{-\left(\frac{t-t_0}{\tau}\right)^2}, \tag{10}$$

where

$$\tau = 5.0035 \times 10^{-10} s, \quad t_0 = 4.5\tau, \quad M = 1.$$

To further evaluate the performance of the proposed method, comparisons were conducted with the harmonic mean conformal FDTD (HM-CFDTD), arithmetic mean conformal FDTD (AM-CFDTD), and Computer Simulation Technology (CST) method simulation results. Fig. 6 presents the sampled values of the electric field $E_x$ at a point 30 mm above the copper sphere. The overall distribution and magnitude obtained using the three methods were in close agreement, demonstrating the accuracy of the harmonic-mean-based conformal approach.

Figures 7 and 8 show the radar cross sections (RCS) of the copper sphere in the $x$-$z$ and $x$-$y$ planes, respectively. The RCS results obtained using the three methods were in excellent agreement. While Fig. 6 demonstrates strong consistency in the near-field results, Fig. 7 and Fig. 8 further confirm the accuracy of the far-field predictions.

Table 1 compares the memory usage and computational time of the HM-CFDTD, arithmetic AM-CFDTD, and CST methods. The HM-CFDTD and AM-CFDTD methods exhibited comparable memory consumption and computational costs. Notably, the harmonic mean-based conformal method requires only 60% of the computational time and 36% of the memory

**TABLE 1**. Comparison of time and memory consumption for the three methods.

| Method | Grid | Execution time | Memory |
|---|---|---|---|
| HM-CFDTD | 15 mm | 1.6894 min | 846 MB |
| AM-CFDTD | 15 mm | 1.7332 min | 852 MB |
| CST | 15 mm | 2.9800 min | 2350 MB |

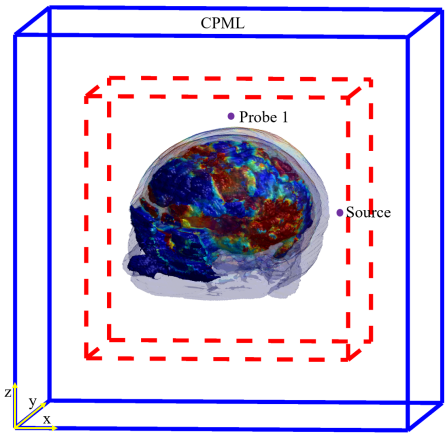


**FIGURE 9**. Human head model.

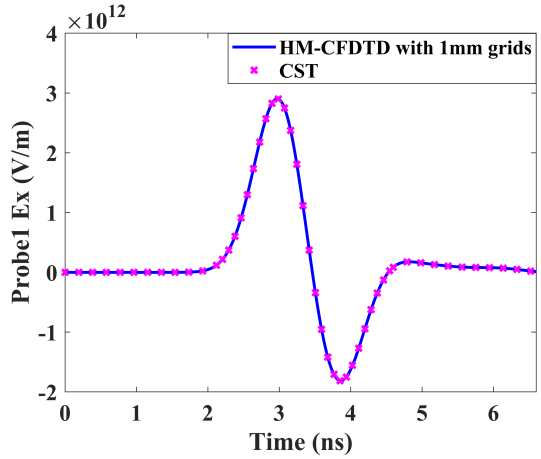


**FIGURE 10**. Time-domain variation of the electric field component $E_x$.

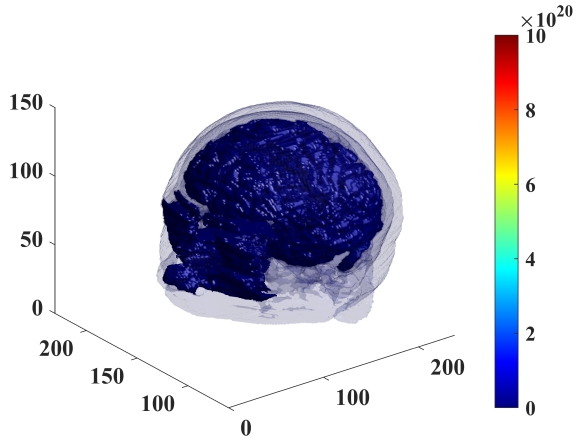


**FIGURE 11**. Distribution of SAR in the human head at 0.9629 ns (unit: W/kg).

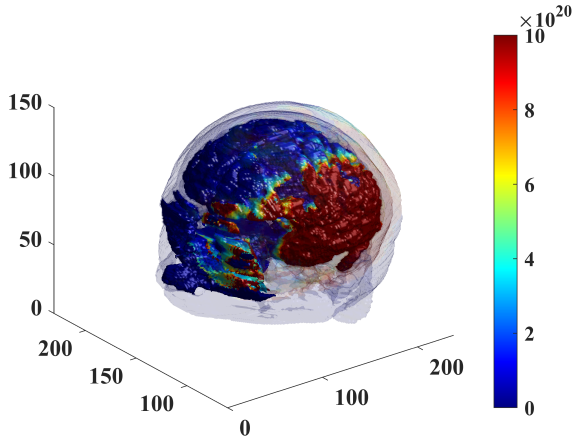


**FIGURE 12**. Distribution of SAR in the human head at 1.9258 ns (unit: W/kg).

compared to the CST, demonstrating its computational efficiency.

To further quantify and evaluate the differences, we adopt the $L_2$-norm error, a standard metric in electromagnetics, as defined in (11). As shown in Fig. 6, the $L_2$-norm error between the $E_x$ field obtained using the HM-CFDTD method and that computed by CST is 1.14%. In comparison, the corresponding $L_2$-norm error between the AM-CFDTD method and CST is 1.12%. These results indicate that the proposed HM-CFDTD method achieves a satisfactory level of accuracy.

$$L_2\text{-norm Error} = \frac{1}{N}\sum_{i=1}^{N}(y_1 - y_2)^2, \tag{11}$$

where $N$ denotes the total number of sampling points, $y_1$ the results obtained using the HM-CFDTD or AM-CFDTD methods, and $y_2$ the results computed by CST.

### 3.2. Human Head Model

To evaluate the effectiveness of the proposed HM-CFDTD method in simulating complex geometries, a human head model was employed, as depicted in Fig. 9. The computational domain was discretized into a grid of $299 \times 299 \times 171$ cells with a uniform spatial resolution of 1 mm × 1 mm × 1 mm. A 10-cell CPML was applied at the boundaries. The electromagnetic parameters of the human head are presented in Table 2. Owing to the complexity of the model, only the major tissue parameters are included in the table.

**TABLE 2**. Electromagnetic parameters of human head tissues.

| Tissue | $\varepsilon_r$ | $\sigma$ | $\mu$ | $\rho$ |
|---|---|---|---|---|
| Muscle | 52.7 | 1.73 | 1.0 | 1050 |
| Eye | 68.7 | 1.53 | 1.0 | 1005 |
| Bone | 20.8 | 0.14 | 1.0 | 1800 |
| Cerebrum | 50.4 | 0.98 | 1.0 | 1040 |
| Cerebellum | 49.0 | 0.90 | 1.0 | 1045 |
| Cerebrospinal Fluid | 68.6 | 2.41 | 1.0 | 1007 |
| Fat | 5.28 | 0.10 | 1.0 | 920 |

The simulation was excited using a point source, and the excitation signal was defined by (12). The excitation source is placed adjacent to the right ear of the human head model, at the center of a plane located 38 grid cells from the CPML boundary. Electric field sampling is conducted directly above the

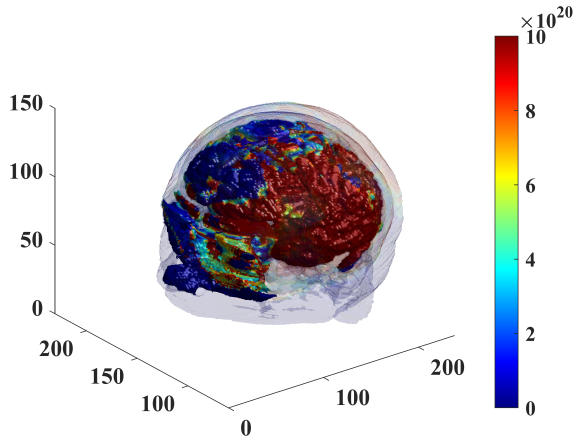


**FIGURE 13**. Distribution of SAR in the human head at 2.8887 ns (unit: W/kg).

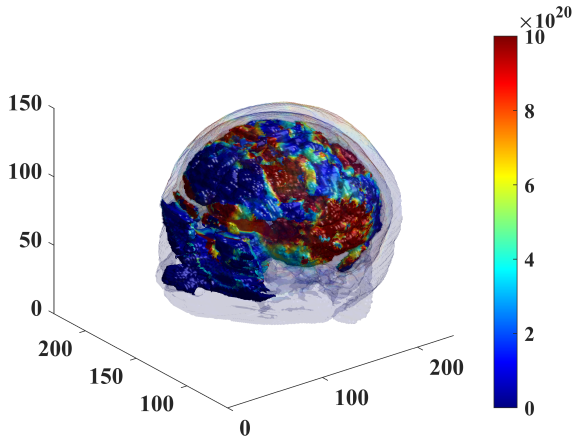


**FIGURE 14**. Distribution of SAR in the human head at 3.8516 ns (unit: W/kg).

head, and the simulation results are benchmarked against those obtained from CST. Fig. 10 presents the time-domain evolution of the $E_x$ field component calculated using both the HM-CFDTD method and CST. The close agreement between the two sets of results validates the accuracy and robustness of the HM-CFDTD approach for modeling complex anatomical structures.

$$E(t) = A\frac{t-t_0}{t_1}e^{-\left(\frac{t-t_0}{t_1}\right)^2}, \tag{12}$$

where $t$ denotes the time, with $t_1 = 0.53$ ns and $t_0 = 4t_1$. The amplitude $A$ is $4.0967 \times 10^{17}$.

To investigate the effects of electromagnetic fields on the human head, the specific absorption rate (SAR) was calculated in this study. SAR is a metric used to quantify the rate at which electromagnetic energy is absorbed by the biological tissues. The SAR is given in (13) [15].

$$\text{SAR} = \frac{\sigma|E|^2}{\rho}, \tag{13}$$

where $\rho$ denotes the density, and $\mathbf{E}$ is the electric field vector. This definition differs from the 1 g/10 g averaged SAR used in regulatory safety standards.

The time evolution of the SAR computed using the proposed HM-CFDTD method is shown in Figs. 11–14. It can be observed that the SAR distribution in the human head varies over time with the propagation of electromagnetic waves.

## 4. CONCLUSION

This study proposes a harmonic mean-based weighting approach for electromagnetic parameters to achieve a conformal implementation. The proposed method eliminates the need to distinguish between dielectric and PEC conformal treatments, thereby avoiding case-dependent formulations and providing a unified framework for conformal modeling. A copper sphere was employed as a benchmark example to verify that the harmonic mean-based conformal method achieves results and accuracy comparable to those obtained using conventional arithmetic-mean weighting. Furthermore, a complex human head model was considered to demonstrate the applicability of the proposed approach to geometrically intricate structures. These results demonstrate that the harmonic mean-based conformal method enables efficient and unified analysis of complex multi-material scenarios, providing a solid foundation for practical RF/microwave device design and bioelectromagnetic simulations.

## ACKNOWLEDGEMENT

This work was supported in part by the Anhui Provincial Major Science and Technology Projects 18030901002 and the Anhui Province Higher Education Science Research Project under Grant 2022AH050070.

## REFERENCES

[1] Taflove, A. and S. C. Hagness, *Computational Electrodynamics*, 2005.

[2] Niu, K., Z. Huang, M. Li, and X. Wu, "Optimization of the artificially anisotropic parameters in WCS-FDTD method for reducing numerical dispersion," *IEEE Transactions on Antennas and Propagation*, Vol. 65, No. 12, 7389–7394, Dec. 2017.

[3] Holland, R., "Pitfalls of staircase meshing," *IEEE Transactions on Electromagnetic Compatibility*, Vol. 35, No. 4, 434–439, Nov. 1993.

[4] Dey, S. and R. Mittra, "A locally conformal finite-difference time-domain (FDTD) algorithm for modeling three-dimensional perfectly conducting objects," *IEEE Microwave and Guided Wave Letters*, Vol. 7, No. 9, 273–275, Sep. 1997.

[5] Xiao, T. and Q. H. Liu, "Enlarged cells for the conformal FDTD method to avoid the time step reduction," *IEEE Microwave and Wireless Components Letters*, Vol. 14, No. 12, 551–553, Dec. 2004.

[6] Beggs, J. H., R. J. Luebbers, K. S. Yee, and K. S. Kunz, "Finite-difference time-domain implementation of surface impedance boundary conditions," *IEEE Transactions on Antennas and Propagation*, Vol. 40, No. 1, 49–56, Jan. 1992.

[7] Sarto, M. S., "A new model for the FDTD analysis of the shielding performances of thin composite structures," *IEEE Transactions on Electromagnetic Compatibility*, Vol. 41, No. 4, 298–306,

Nov. 1999.

[8] Fujita, K., "Hybrid Newmark-conformal FDTD method for multiphysics modeling of short spark gaps with curved metallic surfaces," *IEEE Journal on Multiscale and Multiphysics Computational Techniques*, Vol. 2, 66–77, 2017.

[9] Xiao, T. and Q. H. Liu, "A 3-D enlarged cell technique (ECT) for the conformal FDTD method," *IEEE Transactions on Antennas and Propagation*, Vol. 56, No. 3, 765–773, Mar. 2008.

[10] Zheng, H., Y. Wu, K. Zhang, L. Wang, M. Wang, and E. Li, "Wide-band modeling on-chip spiral inductors using frequency-dependent conformal ADI-FDTD method," *IEEE Access*, Vol. 7, 184 940–184 949, 2019.

[11] Liu, H., X. Zhao, X.-H. Wang, S. Yang, and Z. Chen, "An unconditionally stable conformal LOD-FDTD method for curved PEC objects and its application to EMC problems," *IEEE Transactions on Electromagnetic Compatibility*, Vol. 64, No. 3, 827–839, Jun. 2022.

[12] Hu, X.-J. and D.-B. Ge, "Study on conformal FDTD for electromagnetic scattering by targets with thin coating," *Progress In Electromagnetics Research*, Vol. 79, 305–319, 2008.

[13] Ni, J., X. Han, Q. Lu, and S. Liu, "Simulation of borehole radar responses to rough fractures based on 3-D conformal FDTD," *IEEE Transactions on Geoscience and Remote Sensing*, Vol. 60, 1–15, 2022.

[14] Gabriel, C., S. Gabriel, and E. Corthout, "The dielectric properties of biological tissues: I. Literature survey," *Physics in Medicine & Biology*, Vol. 41, No. 11, 2231–2249, 1996.

[15] Zhang, H. H., Z. C. Lin, W. E. I. Sha, W. W. Choi, K. W. Tam, D. G. Donoro, and G. Shi, "Electromagnetic-thermal analysis of human head exposed to cell phones with the consideration of radiative cooling," *IEEE Antennas and Wireless Propagation Letters*, Vol. 17, No. 9, 1584–1587, Sep. 2018.